

Vascularized and functional human liver from an iPSC-derived organ bud transplant

Takanori Takebe^{1,2}, Keisuke Sekine¹, Masahiro Enomura¹, Hiroyuki Koike¹, Masaki Kimura¹, Takunori Ogaeri¹, Ran-Ran Zhang¹, Yasuharu Ueno¹, Yun-Wen Zheng¹, Naoto Koike^{1,3}, Shinsuke Aoyama⁴, Yasuhisa Adachi⁴ & Hideki Taniguchi^{1,2}

A critical shortage of donor organs for treating end-stage organ failure highlights the urgent need for generating organs from human induced pluripotent stem cells (iPSCs)¹. Despite many reports describing functional cell differentiation^{2–4}, no studies have succeeded in generating a three-dimensional vascularized organ such as liver. Here we show the generation of vascularized and functional human liver from human iPSCs by transplantation of liver buds created *in vitro* (iPSC-LBs). Specified hepatic cells (immature endodermal cells destined to track the hepatic cell fate) self-organized into three-dimensional iPSC-LBs by recapitulating organogenetic interactions between endothelial and mesenchymal cells⁵. Immunostaining and gene-expression analyses revealed a resemblance between *in vitro* grown iPSC-LBs and *in vivo* liver buds. Human vasculatures in iPSC-LB transplants became functional by connecting to the host vessels within 48 hours. The formation of functional vasculatures stimulated the maturation of iPSC-LBs into tissue resembling the adult liver. Highly metabolic iPSC-derived tissue performed liver-specific functions such as protein production and human-specific drug metabolism without recipient liver replacement⁶. Furthermore, mesenteric transplantation of iPSC-LBs rescued the drug-induced lethal liver failure model. To our knowledge, this is the first report demonstrating the generation of a functional human organ from pluripotent stem cells. Although efforts must ensue to translate these techniques to treatments for patients, this proof-of-concept demonstration of organ-bud transplantation provides a promising new approach to study regenerative medicine.

Since the discovery of embryonic stem cells in 1981, decades of laboratory studies have failed to generate a complex vascularized organ such as liver from pluripotent stem cells, giving rise to the prevailing belief that *in vitro* recapitulation of the complex interactions among cells and tissues during organogenesis is essentially impractical⁷. Here we challenge this idea by focusing on the earliest process of organogenesis, that is, cellular interactions during organ-bud development.

During early liver organogenesis, newly specified hepatic cells delaminate from the foregut endodermal sheet and form a liver bud⁸, a condensed tissue mass that is soon vascularized. Such large-scale morphogenetic changes depend on the exquisite orchestration of signals between endodermal epithelial, mesenchymal and endothelial progenitors before blood perfusion⁵. These observations led us to propose that three-dimensional liver-bud formation can be recapitulated *in vitro* by culturing hepatic endoderm cells with endothelial and mesenchymal lineages (Fig. 1a). To examine this hypothesis, we first prepared hepatic endoderm cells from human iPSCs (iPSC-HEs) by directed differentiation, producing approximately 80% of the treated cells expressed the hepatic marker HNF4A, which is involved in cell fate determination (Supplementary Fig. 1).

Next, to recapitulate early organogenesis, human iPSC-HEs were cultivated with stromal cell populations; human umbilical vein endothelial cells (HUVECs) and human mesenchymal stem cells (MSCs) unless stated otherwise, because of their primitive nature (Supplementary Fig. 2a and Supplementary Discussion). Notably, although cells were plated in

two-dimensional conditions, human iPSC-HEs self-organized into macroscopically visible three-dimensional cell clusters by an intrinsic organizing capacity up to 48 h after seeding (Fig. 1 b, c, Supplementary

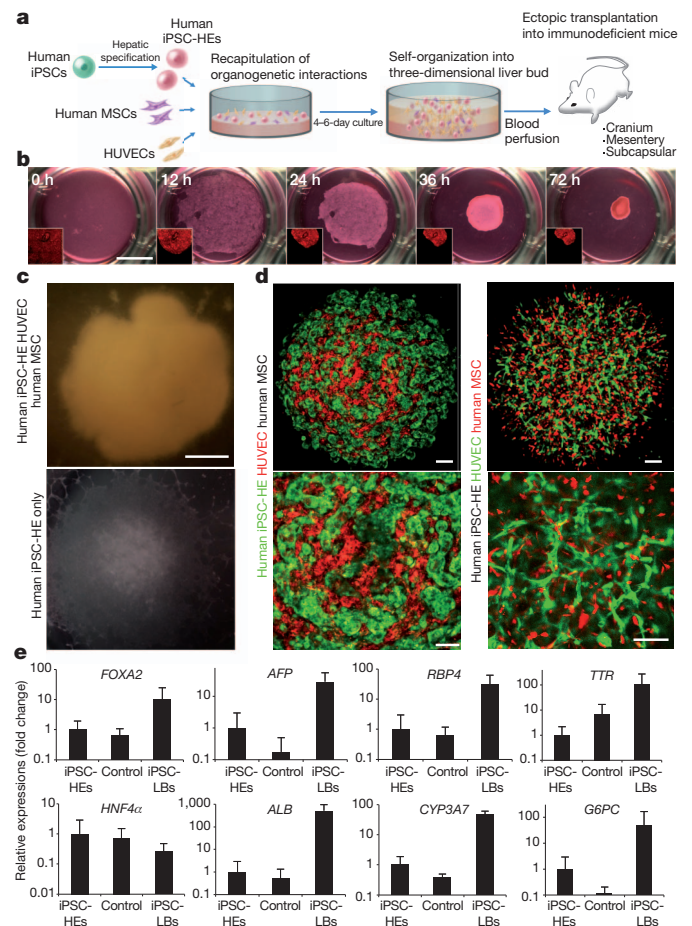


Figure 1 | Generation of human liver buds from human iPSCs. **a**, Schematic representation of our strategy. **b**, Self-organization of three-dimensional human iPSC-LBs in co-cultures of human iPSC-HEs with HUVECs and human MSCs (see also Supplementary Video 1). The time-lapse fluorescence imaging of human iPSC-HEs is shown here. Scale bar, 5 mm. **c**, Gross observation of human iPSC-LBs (top panel) and conventional two-dimensional cultures (bottom panel). Scale bar, 1 mm. **d**, Presence of human iPSC-HEs and nascent endothelial networks inside human iPSC-LBs. Green, human iPSC-HE or HUVEC; red, HUVEC or human MSC. Scale bars, 100 μ m. **e**, Quantitative PCR analysis of hepatic marker gene expression in human iPSC-LBs at day 6 of culture. Control samples were iPSC-HE:HUVEC:humanMSC cells that had been grown as separate cell types and not cultured together, then for control gene expression analysis the cells were mixed together at the same ratio of cell types as in human iPSC-LBs. Results represent mean \pm s.d., $n = 8$.

¹Department of Regenerative Medicine, Yokohama City University Graduate School of Medicine, 3-9 Fukuura, Kanazawa-ku, Yokohama, Kanagawa 236-0004, Japan. ²Advanced Medical Research Center, Yokohama City University, Yokohama, Kanagawa 236-0004, Japan. ³Department of Surgery, Seirei Sakura Citizen Hospital, 2-36-2 Ebaradai, Sakura, Chiba 285-8765, Japan. ⁴ADME & Tox. Research Institute, Sekisui Medical Company Ltd., Tokai, Ibaraki 319-1182, Japan.

Fig. 2b, c and Supplementary Video 1). The presumed human iPSC-derived liver buds (iPSC-LBs) were mechanically stable and could be manipulated physically. We visualized a formation of endothelial network and homogeneously distributed human iPSC-HEs by using fluorescence-labelled cells (Fig. 1d). Although human iPSC-LBs are a tri-lineage mixed tissue and difficult to compare directly with human iPSC-HEs, quantitative polymerase chain reaction (PCR) analysis revealed that cells in human iPSC-LB had significantly increased expression of early hepatic marker genes such as alpha-fetoprotein (*AFP*), retinol binding protein 4 (*RBP4*), transthyretin (*TTR*) and albumin (*ALB*) (Fig. 1e)⁸. Microarray profiling showed that FGF and BMP pathways were upregulated highly in human iPSC-HEs when co-cultured with stromal cells, suggesting the involvement of stromal-cell-dependent factors in liver-bud formation (Supplementary Fig. 3a). Consistent with this, loss- and gain-of-function experiments suggested that, in addition to the direct cell-to-cell interactions, stromal-cell-dependent paracrine support is essential for three-dimensional liver-bud formation through the activating FGF and BMP pathways (Supplementary Fig. 3b–i and Supplementary Discussion)⁹.

Human liver-bud formation is initiated on the third or fourth week of gestation, and this corresponds to embryonic day 9.5 (E9.5) to E10.5 for mouse liver-bud formation¹⁰. Similar to E10.5 mouse liver bud, immunohistochemistry showed that human iPSC-LB is composed of proliferating AFP-positive hepatoblasts¹¹ as well as mesenchymal and endothelial

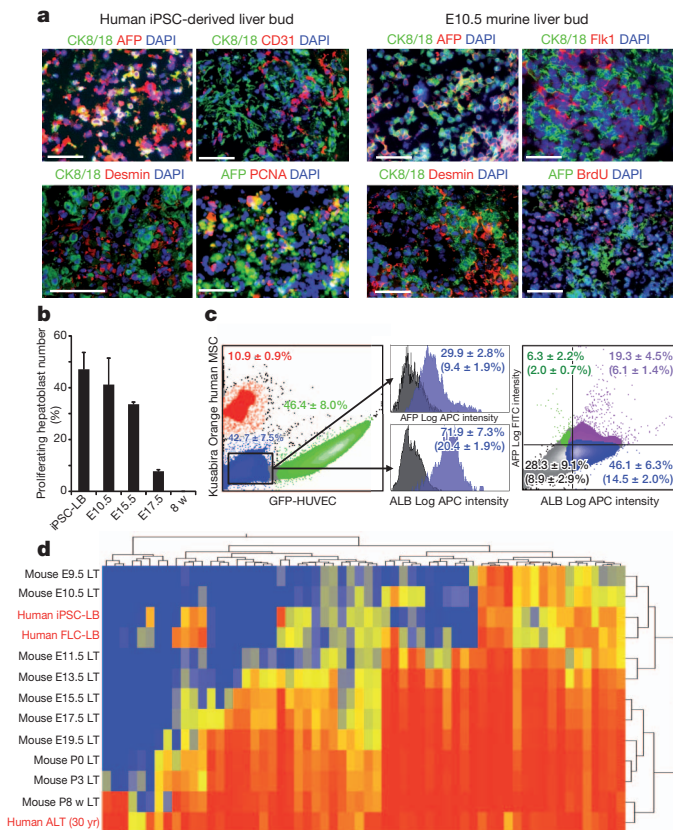


Figure 2 | *In vitro* characterization of human iPSC-LBs. **a**, Immunostaining of CK8/18, AFP, PECAM1 (CD31), FLK1, desmin, PCNA and BrdU (5-bromodeoxyuridine). Scale bars, 100 μ m. **b**, Proportions of proliferating hepatic cells, as assessed by dividing the number of PCNA-positive or BrdU-positive cells by the number of CK8/18-positive cells (shown as a percentage). Results represent means \pm s.d., $n = 3$. **c**, Representative flow cytometry profile showing the average number of AFP-positive and/or ALB-positive human iPSC-HEs at day 4 of culture in six independent differentiation experiments. Human iPSC-HEs were separated from stromal populations by the use of fluorescence labelled cells. Average percentages of the total cells and s.e.m. are given in brackets. **d**, Comparison of liver developmental gene signatures among human iPSC-LB, human FLC-LB, human adult (30 years old) liver tissue (ALT) and mouse liver tissue (LT) of various developmental stages (from E9.5 to 8 weeks after birth).

progenitors (Fig. 2a). Hepatic cells in human iPSC-LBs were as proliferative as E10.5 mouse liver buds (Fig. 2b). Flow cytometric characterization revealed that $42.7 \pm 7.5\%$ ($n = 6$) of cells in human iPSC-LBs were identified as iPSC-HEs using fluorescence-labelled HUVECs and MSCs. Among these, approximately $71.9 \pm 7.3\%$ ($n = 6$) of human iPSC-HEs expressed ALB and $29.9 \pm 2.8\%$ expressed AFP, and $19.3 \pm 4.5\%$ were positive for both ALB and AFP (Fig. 2c).

To characterize the expression profiles of human iPSC-LBs and to compare with those of a corresponding developmental stage, we carried out microarray analysis of 83 selected genes that are serially upregulated during liver development. Hierarchical clustering analyses suggested that the expression profiles of human iPSC-LBs at day 4 of culture resembled those of mouse E10.5 and E11.5 liver buds rather than advanced fetal or adult livers (Fig. 2d). These expression profiles were relatively similar to those of human fetal liver cell-derived liver buds (FLC-LBs) (Fig. 2d), which also have an ability to form LBs (Supplementary Figs 2a and 4). The 83-gene expression profile of human iPSC-LBs showed closer signatures to more advanced human liver

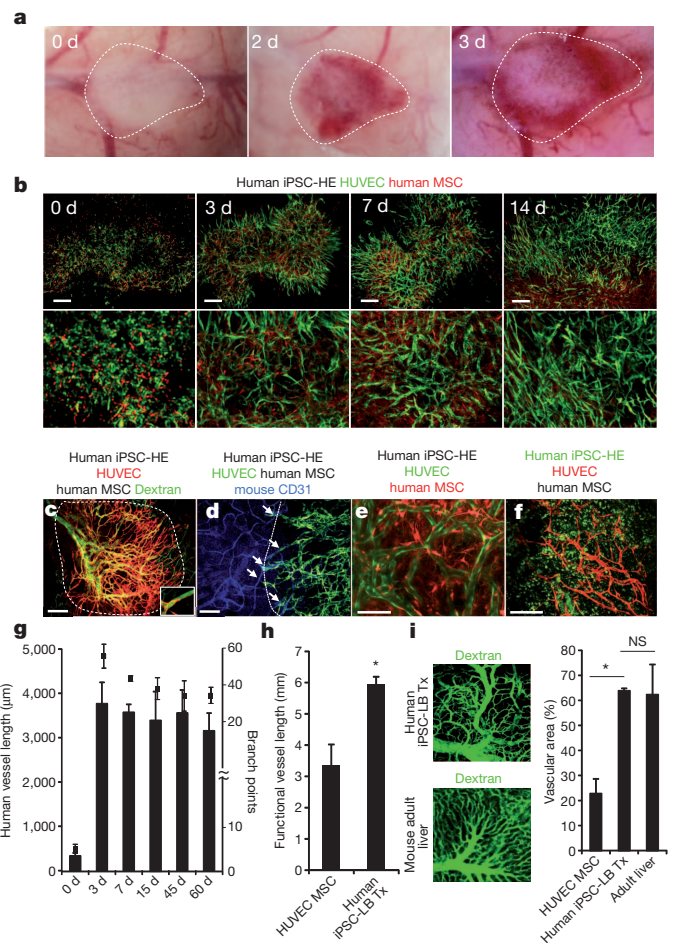


Figure 3 | Generation of human liver with functional vascular networks *in vivo*. **a**, Macroscopic observation of transplanted human iPSC-LBs, showing perfusion of human blood vessels. Dotted area indicates the transplanted human iPSC-LBs. **b**, Intravital tracking of human iPSC-LBs, showing *in vivo* dynamics of vascularization. **c**, Dextran infusion showing the functional human vessel formation at day 3. Scale bar, 500 μ m. **d**, Visualization of the connections (arrows) among HUVECs (green) and host vessels (blue). Scale bar, 250 μ m. **e, f**, Localization of human MSCs or human iPSC-derived cells at day 15. Scale bars, 100 and 250 μ m. **g**, Quantification of human vessels over time (mean \pm s.e.m., $n = 3$). Error bars attached to the bars relate to the left axis (vessel length), error bars attached to squares relate to the right axis (branch points). **h**, Comparison of functional vessel length between human iPSC-LB and HUVEC human MSC transplants (Tx) (mean \pm s.e.m., $n = 5$, $*P < 0.01$). **i**, Vascular networks of human iPSC-LB-derived tissue is similar to that of mouse adult livers (mean \pm s.e.m., $n = 5$, $*P < 0.01$).

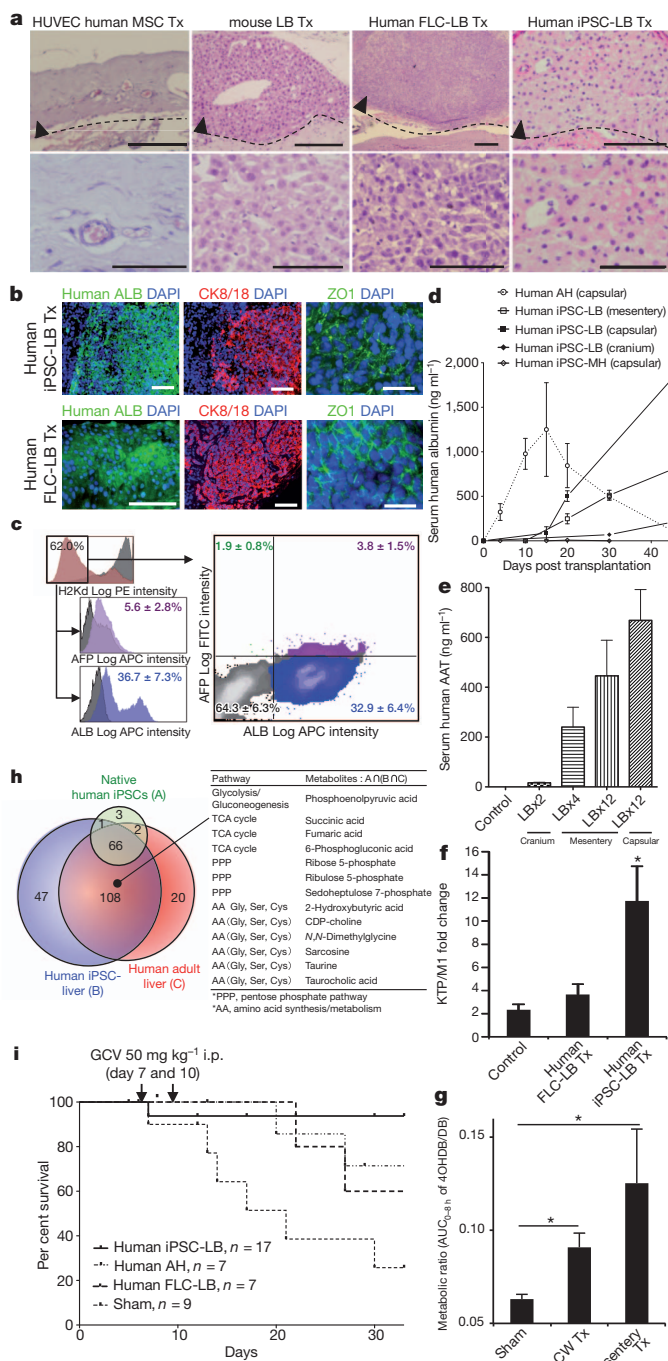


Figure 4 | Functional characterization of human iPSC-LB derived liver.

a, b, Haematoxylin and eosin, and immunofluorescence staining of tissues at day 60. Dotted line indicates the border on the brain. Scale bars, 200 μm (**a**, top row); 100 μm (**a**, bottom row and **b**, left and middle images on top and bottom rows) and 25 μm (**b**, right images, top and bottom rows). **c**, Representative FACS profile for AFP- and/or ALB-positive human cells at day 60 ($n = 8$). Human cells were identified as a murine H2Kd-negative population. Results are shown as contour maps coloured by density of the scatter data. ALB⁻/AFP⁻ population is grey; ALB⁻/AFP⁺ population is green; ALB⁺/AFP⁻ population is blue; and ALB⁺/AFP⁺ population is purple. **d, e**, ELISA showing levels of human serum ALB and AAT over time at various ectopic sites (cranium, mesentery and kidney subcapsule), compared with that of hAH (mean \pm s.e.m., $n = 4$ in **d**, $n = 3$ in **e**). See also Supplementary Tables 2 and 3. **f, g**, Human-specific ketoprofen (**f**) and debrisoquine (**g**) metabolite formations (mean \pm s.e.m., $n = 3$, $*P < 0.05$).

Metabolic ratios were determined by dividing the AUC_{0-8h} (the area under the curve from time 0 until 8 h; detailed explanation is described in Supplementary Methods) ratio of 4-hydroxydebrisoquine (4OHDB) to debrisoquine (DB). **h**, Venn diagram shows the metabolic profiles of human iPSC-LB transplants measured by CE-TOFMS (capillary electrophoresis time-of-flight mass spectrometry) (Supplementary Fig. 18). Representative metabolites are shown. **i**, Kaplan–Meier survival curves of TK-NOG mice after liver injury ($P = 0.0120$). i.p., intraperitoneal.

mouse CD31 antibody, we showed that human blood vessels within the transplant became patent (unobstructed) by connecting host vessels at the edge of the transplant (Fig. 3c, d), and this was confirmed by whole-mount immunostaining of the explants (Supplementary Figs 9 and 10a, b, and Supplementary Video 4). Functional vessel formation was essential for the successful engraftment because human iPSC-HEs transplanted without endothelial cells failed to vascularize and engraft (Supplementary Fig. 10c–f). Human vessels were long-lasting as they were stabilized by human MSC-derived perivascular cells (Fig. 3e–g)^{13,14}. Interestingly, the human iPSC-LB transplant vascular networks were similar in density and morphology to those of adult livers, whereas the vasculature in only HUVECs and human MSC transplants were much less dense; functional vessels were of similar diameter (approximately 12 μm) in both settings (in iPSC-LB transplants, and in HUVEC and human MSC transplants) (Fig. 3h, i, and Supplementary Figs 11 and 12). Animal studies suggest that endothelial cells not only form passive conduits to deliver nutrients and oxygen but also establish an instructive vascular niche, which stimulates liver organogenesis and regeneration through elaboration of paracrine trophogens^{5,15}. Our transplantation approach provided a unique intravital monitoring system for evaluating human iPSC-derived organ maturation and differentiation throughout the organogenesis, enabling us to dissect the previously uncharacterized roles of stromal cell types in human organ development.

The liver-bud transplants were examined histologically at multiple time points. Hepatic cells in human iPSC-LBs proliferated rigorously, particularly until 2 months after transplantation (Supplementary Fig. 13). Similar to human FLC-LBs, human iPSC-LB transplants consisted of hepatic cord-like structures characteristic of adult liver after 60 days (Fig. 4a), composed of cells expressing the tight junction protein zona occludens 1 (ZO1), ALB and CK8/18 (Fig. 4b), asialoglycoprotein receptor 1 (ASGR1) and collagen IV (Supplementary Fig. 14), which were normally found along the entire length of the sinusoid¹⁶. AFP-negative transplant-derived hepatic cells had the ultrastructural features of mature hepatocytes (Supplementary Fig. 15a–e). Quantitative fluorescence-activated cell sorting (FACS) profiling of human iPSC-LB transplants showed that 32.9 \pm 6.4% ($n = 8$) of the total human cells were positive for just ALB, whereas 3.8 \pm 1.5% were positive for both ALB and AFP, as seen in human FLC-LB transplants, suggesting the maturation of human iPSC-HEs (Fig. 4c and Supplementary Fig. 16).

To evaluate the functional maturation of human iPSC-LB ectopic transplants compared with that of human adult hepatocytes, human serum albumin was tracked by ELISA. Four transplanted human iPSC-LBs (consisting 1.8 $\times 10^5$ immature hepatic cells) began producing albumin at approximately day 10 and produced up to 1,983 ng ml⁻¹ by day 45, and hepatic maturation was observed at iPSC-LBs transplanted at various ectopic sites, whereas 4 $\times 10^6$ human adult hepatocytes could not keep producing high levels of albumin and showed a peak at

tissues derived from fetuses and adults 22 to 40 weeks into gestation than did human iPSC-derived mature hepatocyte-like cells (human iPSC-MHs) induced by published protocols⁴. This reflects the efficient hepatic commitment in liver buds as they mimicked ontogenetic interactions consistent with higher albumin production capacity after extended culture (Supplementary Figs 5 and 6).

Haemodynamic stimulation is essential for liver-bud maturation¹². To test whether human iPSC-LBs were capable of generating completely functional liver, we used a cranial window model because of the optical access¹³. We first tested the feasibility of this model by using mouse liver-bud-derived cells (Supplementary Discussion and Supplementary Fig. 7). To track the *in vivo* fate of transplanted cells, we performed repeated live imaging of liver-bud transplant-derived tissue over time. Notably, *in vitro*-derived human iPSC-LBs connected quickly with host vasculature within 48 h of transplantation (Fig. 3a, b, Supplementary Fig. 8 and Supplementary Videos 2 and 3). By infusing fluorescein-conjugated dextran and

day 15 (Fig. 4d). Notably, transplanted conventional human iPSC-MHs (1×10^7 cells per mouse) produced much less albumin, suggesting the importance of three-dimensional and vascularized tissue formation for successful engraftment and maturation at ectopic sites. The amount of human serum alpha-1-antitrypsin (AAT) was in proportion to the number of liver-bud transplants (Fig. 4e). Gene-expression profiling of human iPSC-LBs explanted 60 days ($n = 8$) after transplantation demonstrated the significant hepatic maturation compared with conventional human iPSC-MHs ($n = 8$)⁴ (Supplementary Fig. 17).

To analyse the drug metabolism activity that is a major function of the liver, the mice were challenged with ketoprofen¹⁷ or debrisoquine¹⁸, which are known to be metabolized differently by mice and humans. After the drug exposure, formation of human-specific metabolites was demonstrated in urine and serum samples collected from mice transplanted with human iPSC-LBs (Fig. 4f, g and Supplementary Discussion). Furthermore, to characterize the profiles of small-molecule metabolites such as the products of sugar, amino acid and nucleotide metabolism, metabolome analysis of human iPSC-LB transplants was performed. This showed 222 metabolites, including liver-specific metabolites such as taurocholic acid (Fig. 4h). This profile, with a high number of metabolites, was similar to that of human adult liver but not to that of original human iPSCs (Supplementary Fig. 18). These results demonstrate the potential for predicting drug metabolite profiles of humans, with drug metabolite profiles of mice transplanted with human iPSC-LBs mimicking *in vivo* human physiology. This is particularly striking, as successful detection of human drug responsiveness relies on the use of high-quality hepatocytes and severely damaged host liver using conventional chimaeric mouse models^{19,20}.

With an aim to further our understanding of clinical transplantation and its future use, we evaluated the possibility of a minimally invasive mesenteric transplantation model, which would be a more realistic target site. Macroscopic observation confirmed the successful engraftment of transplanted LBs on mesentery (Supplementary Fig. 19a, b). Transplantation of 12 human iPSC-LBs improved the survival of TK-NOG mice²¹ after the gancyclovir-induced liver failure compared with the sham-operated, human FLC-LB- and human adult-hepatocyte-transplanted mice (Fig. 4i and Supplementary Discussion). Thus, we successfully generated vascularized and functional human liver by transplantation of human iPSCs-LBs.

Manipulation of iPSCs holds great promise for regenerative medicine. However, clinical trials of cell transplantation, currently an important target of the stem-cell-based approach, have presented unsatisfactory results²². Our study demonstrates a proof-of-concept that organ-bud transplantation offers an alternative approach to the generation of a three-dimensional, vascularized organ. These results highlight the enormous therapeutic potential using *in vitro*-grown organ-bud transplantation for treating organ failure.

METHODS SUMMARY

Hepatic differentiation of human iPSCs was achieved based on a protocol reported previously⁴. HUVECs and human MSCs (Lonza) were maintained in endothelial growth medium (Lonza) or MSC growth medium (Lonza) at 37 °C in a humidified 5% CO₂ incubator. To generate human liver buds *in vitro*, 1×10^6 human iPSC-derived hepatic cells, 0.8×10^6 to 1×10^6 HUVECs and 2×10^5 human MSCs were resuspended in the mixture of EGM and hepatocyte culture medium (Cambrex) containing with dexamethasone (0.1 μM, Sigma-Aldrich), oncostatin M (10 ng ml⁻¹, R&D System), hepatocyte growth factor (HGF; 20 ng ml⁻¹, PromoKine) and SingleQuots (Lonza) and plated on pre-solidified $\times 2$ Matrigel diluted with EGM (BD Biosciences) in a 24-well plate. After approximately 4 to 6 days of culture, self-organized human iPSC-LBs were detached, collected and transplanted into a pre-formed cranial window¹³ of an immunodeficient mouse.

Full Methods and any associated references are available in the online version of the paper.

Received 18 April 2012; accepted 7 May 2013.

Published online 3 July 2013.

1. Klein, A. S. *et al.* Organ donation and utilization in the United States, 1999–2008. *Am. J. Transplant.* **10**, 973–986 (2010).

2. Kriks, S. *et al.* Dopamine neurons derived from human ES cells efficiently engraft in animal models of Parkinson's disease. *Nature* **480**, 547–551 (2011).
3. Kroon, E. *et al.* Pancreatic endoderm derived from human embryonic stem cells generates glucose-responsive insulin-secreting cells *in vivo*. *Nature Biotechnol.* **26**, 443–452 (2008).
4. Si-Tayeb, K. *et al.* Highly efficient generation of human hepatocyte-like cells from induced pluripotent stem cells. *Hepatology* **51**, 297–305 (2010).
5. Matsumoto, K., Yoshitomi, H., Rossant, J. & Zaret, K. S. Liver organogenesis promoted by endothelial cells prior to vascular function. *Science* **294**, 559–563 (2001).
6. Espejel, S. *et al.* Induced pluripotent stem cell-derived hepatocytes have the functional and proliferative capabilities needed for liver regeneration in mice. *J. Clin. Invest.* **120**, 3120–3126 (2010).
7. Kobayashi, T. *et al.* Generation of rat pancreas in mouse by interspecific blastocyst injection of pluripotent stem cells. *Cell* **142**, 787–799 (2010).
8. Zhao, R. & Duncan, S. A. Embryonic development of the liver. *Hepatology* **41**, 956–967 (2005).
9. Si-Tayeb, K., Lemaigre, F. P. & Duncan, S. A. Organogenesis and development of the liver. *Dev. Cell* **18**, 175–189 (2010).
10. Gouysson, G. *et al.* Relationship between vascular development and vascular differentiation during liver organogenesis in humans. *J. Hepatol.* **37**, 730–740 (2002).
11. Jung, J., Zheng, M., Goldfarb, M. & Zaret, K. S. Initiation of mammalian liver development from endoderm by fibroblast growth factors. *Science* **284**, 1998–2003 (1999).
12. Korzh, S. *et al.* Requirement of vasculogenesis and blood circulation in late stages of liver growth in zebrafish. *BMC Dev. Biol.* **8**, 84 (2008).
13. Koike, N. *et al.* Tissue engineering: creation of long-lasting blood vessels. *Nature* **428**, 138–139 (2004).
14. Takebe, T. *et al.* Generation of functional human vascular network. *Transplant. Proc.* **44**, 1130–1133 (2012).
15. Ding, B. S. *et al.* Inductive angiocrine signals from sinusoidal endothelium are required for liver regeneration. *Nature* **468**, 310–315 (2010).
16. Martinez-Hernandez, A. The hepatic extracellular matrix. I. Electron immunohistochemical studies in normal rat liver. *Lab. Invest.* **51**, 57–74 (1984).
17. Ishizaki, T. *et al.* Pharmacokinetics of ketoprofen following single oral, intramuscular and rectal doses and after repeated oral administration. *Eur. J. Clin. Pharmacol.* **18**, 407–414 (1980).
18. Yu, A. M., Idle, J. R. & Gonzalez, F. J. Polymorphic cytochrome P450 2D6: humanized mouse model and endogenous substrates. *Drug Metab. Rev.* **36**, 243–277 (2004).
19. Katoh, M. *et al.* *In vivo* drug metabolism model for human cytochrome P450 enzyme using chimeric mice with humanized liver. *J. Pharm. Sci.* **96**, 428–437 (2007).
20. Kamimura, H. *et al.* Assessment of chimeric mice with humanized liver as a tool for predicting circulating human metabolites. *Drug Metab. Pharmacokinet.* **25**, 223–235 (2010).
21. Hasegawa, M. *et al.* The reconstituted 'humanized liver' in TK-NOG mice is mature and functional. *Biochem. Biophys. Res. Commun.* **405**, 405–410 (2011).
22. Dudley, S. C. Jr. Beware of cells bearing gifts: cell replacement therapy and arrhythmic risk. *Circ. Res.* **97**, 99–101 (2005).

Supplementary Information is available in the online version of the paper.

Acknowledgements We thank F. Kawamata, E. Yoshizawa, Y. Suzuki, S. Nakai, Y. Takahashi, N. Tsuchida and N. Sasaki for kindly providing technical support; J. Nakabayashi, K. Yasumura, R. Fujiwara, T. Amiya, A. Nakano, Y. Mitsuhashi and all of the members of our laboratory for help with several experiments and comments. We are also grateful to D. Fukumura, Y. Goshima, T. Hirose, M. Ichino, U. Yokoyama, T. Ogawa and R. K. Jain for critical evaluation of the manuscript. This work was supported by grants to H. Taniguchi from the Strategic Promotion of Innovative Research and Development (S-innovation, 62890004) of the Japan Science and Technology Agency (JST). This work was also supported by the Grants-in-Aid of the Ministry of Education, Culture, Sports, Science, and Technology of Japan to T. Takebe (no. 24106510, 24689052), N. Koike (no. 22390260) and H. Taniguchi (no. 21249071, 25253079); by the Specified Research Grant of the Takeda Science Foundation and a grant from the Japan IDDM network to H. Taniguchi; and by a grant of the Yokohama Foundation for Advanced Medical Science to T. Takebe.

Author Contributions T.T. conceived the study, performed the experiments, collected and analysed the data and drafted the manuscript. K.S., M.E., H.K., M.K., T.O., R.R.Z. and S.A. performed the experiments with the technical guidance and expertise of K.S., Y.-W.Z., Y.U. and T.T. K.S., Y.-W.Z., N.K., Y.A. and H.T. provided critical advice on the research strategy and design.

Author Information Microarray data, including that of human iPSC-LBs, human FLC-LBs, human adult liver tissues (ALT) and mouse liver tissue of various developmental stages, have been deposited in the Gene Expression Omnibus under accession number GSE46631. Reprints and permissions information is available at www.nature.com/reprints. The authors declare no competing financial interests. Readers are welcome to comment on the online version of the paper. Correspondence and requests for materials should be addressed to T.T. (ttakebe@yokohama-cu.ac.jp) or H.T. (rtanigu@yokohama-cu.ac.jp).

METHODS

Cell culture and differentiation. TkDA3 human iPSC clone used in this study was kindly provided by K. Eto and H. Nakauchi. Undifferentiated human iPSCs were maintained on the mouse embryonic fibroblast cells as feeder cells in human iPSC medium. For endodermal differentiation, human iPSCs were seeded on a Matrigel-coated dish and the medium was changed to RPMI1640 with 1% B27 without insulin and human activin A (100 ng ml^{-1}) for 5 to 6 days. For hepatic specification, human iPSC-derived endodermal cells were treated further with RPMI1640 with 1% B27 and human basic FGF (10 ng ml^{-1}), human BMP4 (20 ng ml^{-1}) for 3 to 4 days. Recombinant human activin A was kindly provided by Y. Eto at Ajinomoto Co. Human FLCs (CS-ABI-3716; Applied Cell Biology Research Institute) were plated on collagen IV-coated 6-well plates (BD Biosciences) and cultured in our standard medium (1:1 mixture of DMEM and F-12 (Sigma Aldrich) supplemented with 10% FBS (lot 7219F; ICN Biochemical), 50 mmol l^{-1} HEPES (Wako Pure Chemical Industries), 2 mmol l^{-1} L-glutamine (Life Technologies Corporation), 50 mmol l^{-1} 2-mercaptoethanol (Sigma), $1 \times$ penicillin-streptomycin (Life Technologies), 10 mmol l^{-1} nicotinamide (Sigma), $1 \times 10^{-4} \text{ M}$ Dexamethasone (Sigma) and $1 \mu\text{g ml}^{-1}$ insulin (Wako)). Human recombinant HGF (50 ng ml^{-1}) and EGF (20 ng ml^{-1}) (Sigma) were added before cultivation. HUVECs and human MSCs (Lonza) were maintained in endothelial growth medium or MSC growth medium (Lonza) at 37°C in a humidified 5% CO_2 incubator. Cryopreserved human adult hepatocytes (lots 582, 737, 746 and HC2-8) were purchased from Xenotech (Lenexa). Human adult hepatocytes were thawed, and the number of viable cells was counted according to the manufacturer's instructions and used for transplantation experiments. *In vitro* albumin production tests were performed on viable cells just after first 24 h of culture.

Retroviral transduction. For live imaging, cells were infected with retroviruses expressing EGFP or human Kusabira-Orange (KO1) as described¹³. In brief, a retrovirus vector *pGCDNsam IRES-EGFP* or *KOFP* was transfected into 293 gag/pol (gp) and 293gpg (gp and VSV-G) packaging cells (kindly provided by M. Onodera) in which viral particle production is induced using a tetracycline-inducible system. Culture supernatants of retrovirus-infected cells were passed through a $0.45\text{-}\mu\text{m}$ filter (Whatman, GE Healthcare) and used immediately for infection. KOFP displays a major absorption wavelength maximum at 548 nm with a slight shoulder at 515 nm and emits a bright orange fluorescence, with a peak at 561 nm.

Transplantation. *In vitro*-generated liver buds were detached, collected and transplanted into a pre-formed cranial window or indicated sites of a non-obese diabetic/severe combined immunodeficient (NOD/SCID) mouse (Sankyo Lab. Co.). The *in vivo* fate of transplanted cells was monitored by intravital imaging using a fluorescence microscope (model BZ-9000; Keyence) or the Leica TCS SP5 confocal microscope (Leica Microsystems). For survival curves, TK-NOG mice (body weights of approximately 20 to 30 g) were used in this study (supplied by the Central Institute for Experimental Animals)²¹. Ganciclovir (50 mg kg^{-1} , intraperitoneal), a drug that is not toxic to human or mouse tissues, was administered to induce tissue-specific ablation of transgenic liver parenchymal cells at day 7 and 10 after a dozen human iPSC-LBs were transplanted on the mesentery. For control experiments, we thawed and isolated the viable human adult hepatocytes, and resuspended the viable cells (3×10^6 to 4×10^6) in cold medium and cold Matrigel (BD) and transplanted them into the kidney subcapsular space. The mice were bred and maintained according to the Yokohama City University institutional guidelines for the use of laboratory animals.

Intravital imaging. Tail vein injections of 1% tetramethylrhodamine-conjugated dextran (2,000,000 MW), fluorescein-isothiocyanate-conjugated dextran (2,000,000 MW) and Texas-Red-conjugated dextran (70,000 MW, neutral) were used to identify vessel lumens (all from Invitrogen). Host endothelial cells were visualized using Alexa647-conjugated mouse-specific CD31 (BD), injected intravitaly. Confocal image stacks were acquired for the implanted vessels and dextran. Image projections were processed using MetaMorph Angiogenesis Module software (Molecular Devices). Total tubule length, the percentage of tubules per field (area of tubules divided by the area of the transplants that were imaged) and tube diameter were then logged automatically into an Excel spreadsheet.

Gene-expression analysis. Quantitative PCR analyses were conducted as described previously²³. Total RNA of human fetal liver (lot no. A601605) and human adult liver (lot no. B308121) were obtained from Biochain Institute (Hayward).

Microarray and data analysis. Total RNA was prepared from human iPSC-derived cells or tissues (human iPSC-LBs, human FLC-LBs), human adult liver tissue and CD45-negative and Ter119-negative murine liver cells at various different developmental stages (E9.5, E10.5, E11.5, E13.5, E15.5, E17.5, E19.5, postnatal day 0 (P0), P3 and postnatal week 8) using an RNeasy Mini Kit (Qiagen). RNA for gene-expression profiling was hybridized on a Whole Human Genome Agilent $4 \times 44\text{K v2}$ Oligonucleotide Microarray or Whole Mouse Genome Agilent $4 \times 44\text{K v2}$ Oligonucleotide Microarray (Agilent Technologies) according to the manufacturer's instructions. To perform cross-species comparison of expression profiles, 26,153 expression data at gene level were cross-referenced to other species using the HomoloGene IDs in the MGI curated data set of human-mouse orthology with Phenotype Annotations (<http://www.informatics.jax.org>). To generate the heat map, we used a hierarchical clustering method with Euclidean distance complete linkage on GeneSpring11.5.1. to analyse the 83 originally selected liver signature gene-expression profiles. Of all genes, 83 genes were selected as liver signature genes because they increased continuously during both murine and human liver development.

ELISA. Blood samples were allowed to clot in a centrifuge tube (approximately 5 min) at room temperature (24°C), loosened from the sides of the tube and kept at 4°C (melting ice) for 20 min. Clotted blood was centrifuged for 10 to 15 min at 400g, 4°C and the serum fraction was removed, taking care to exclude erythrocytes or clotted materials. Human ALB and AAT in the mouse serum samples was measured using a Human Albumin ELISA Quantitation Kit (Bethyl Laboratories) and human alpha 1-antitrypsin ELISA Quantitation Kit (GenWay Biotech) according to the manufacturer's instructions.

Whole mount immunostaining. Mice were perfused with 4% paraformaldehyde in phosphate buffer solution (PBS) through cardiac puncture. The cover-glass forming the cranial window was removed, and the transplants (approximately $300\text{-}\mu\text{m}$ thick) were extracted and placed in 4% paraformaldehyde in PBS for 1.5 h on ice. For immunostaining, fixed collagen gels were washed three times in PBS (10 min each), blocked with 3% BSA or 0.1% Triton X-100 for 1 h, incubated with primary antibodies at 4°C overnight, followed by three 10-min washes in PBS or 0.1% Triton X-100. The sample was incubated with secondary antibodies at 4°C overnight, followed by three 10-min washes in PBS or 0.1% Triton X-100. Tissue samples were counterstained with DAPI and mounted on glass slides in mounting media (Vector Laboratories), under a cover slip. The following primary antibodies were used: mouse anti-human ZO1, mouse anti-human CD31 and rat anti-mouse CD31 (BD Biosciences), rabbit anti-mouse collagen IV (Millipore) and desmin (Dako Corporation). Immunostaining was analysed using the Leica TCS SP5 confocal microscope.

Tissue processing and immunostaining. Tissues were fixed overnight at 4°C in 4% paraformaldehyde, processed, and embedded in paraffin. Transverse sections ($4 \mu\text{m}$) were placed on MAS-coated slides (Matsunami) for immunostaining or standard histological staining with haematoxylin and eosin. Immunostaining was preceded by autoclave antigen retrieval in citrate buffer (pH 6.0). The primary antibodies were anti-human: CD31, smooth muscle actin, AFP, CK8/18 (all from Dako Corporation) and ALB (BD Biosciences). Tissue sections were incubated with secondary antibody Alexa Fluor (Life Technologies) for 1 h at room temperature, followed by DAPI (Sigma) nuclear staining. The images were acquired using the LSM510 laser scanning microscope (Carl Zeiss).

Statistical analysis. Data are expressed as the means \pm s.d. or s.e.m. from at least three independent experiments. Comparisons between three or four groups were analysed using the Wilcoxon statistical analyses or Kruskal-Wallis test by ranks, and post-hoc comparisons were made using the Mann-Whitney *U*-test with Bonferroni correction. Two-tailed *P* values of <0.05 were considered significant.

- Kobayashi, S. *et al.* Reconstruction of human elastic cartilage by a CD44⁺ CD90⁺ stem cell in the ear perichondrium. *Proc. Natl Acad. Sci. USA* **108**, 14479–14484 (2011).